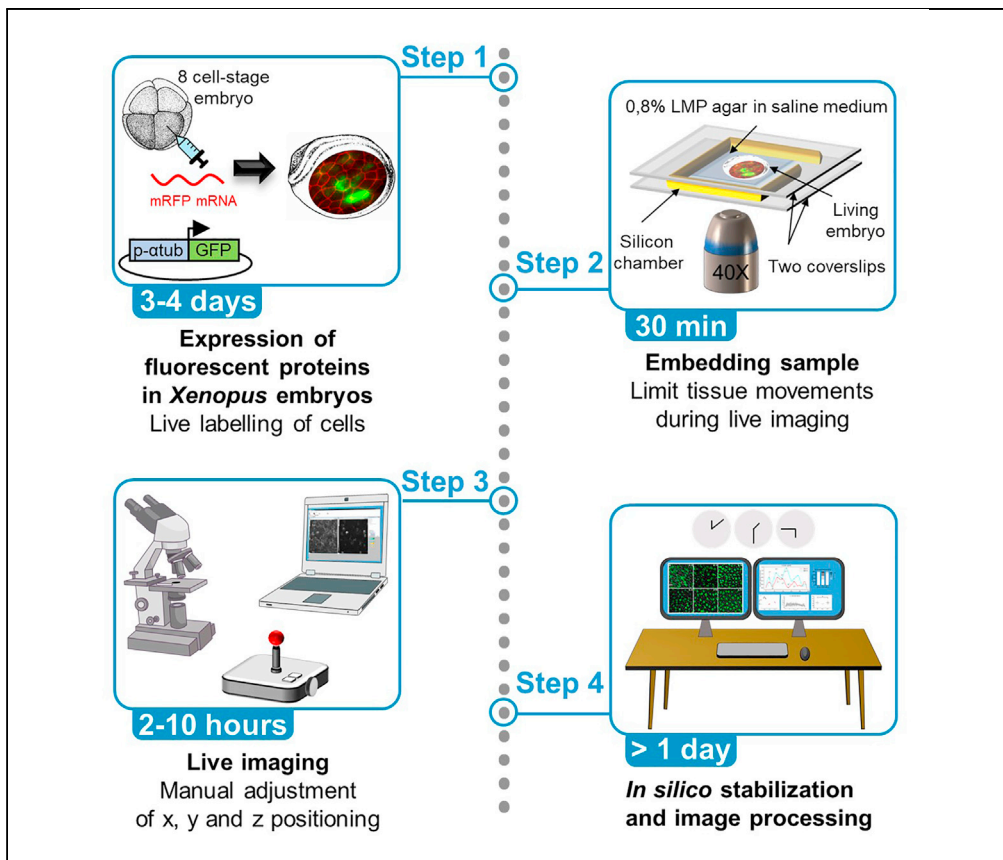# STAR Protocols

Protocol

A live-imaging protocol to track cell movement in the *Xenopus* embryo

Alexandre Chuyen,
Fabrice Daian,
Andrea Pasini,
Laurent
Kodjabachian

andrea.pasini@univ-amu.
fr (A.P.)
laurent.kodjabachian@
univ-amu.fr (L.K.)

Highlights

Tracking of individual
cell movement *in vivo*
during *Xenopus*
embryonic
development

Labeling and tracking
of multiciliated cells
(MSSs) in bilayered
Xenopus epidermis

In silico stabilization
corrects drifting
caused by embryo
morphogenesis

Tracking individual cell movement during development is challenging, particularly in tissues subjected to major remodeling. Currently, most live imaging techniques in *Xenopus* are limited to tissue explants and/or to superficial cells. We describe here a protocol to track immature multiciliated cells (MCCs) moving within the inner epidermal layer of a whole embryo. In addition, we present a data processing protocol to uncouple the movements of individual cells from the coplanar drifts of the tissue in which they are embedded.

Protocol

A live-imaging protocol to track cell movement in the *Xenopus* embryo

Alexandre Chuyen,[1,2] Fabrice Daian,[1] Andrea Pasini,[1,*] and Laurent Kodjabachian[1,3,*]

[1]Aix-Marseille University, CNRS, IBDM, Turing Centre for Living Systems, Marseille, France

[2]Technical contact

[3]Lead contact

*Correspondence: andrea.pasini@univ-amu.fr (A.P.), laurent.kodjabachian@univ-amu.fr (L.K.)
https://doi.org/10.1016/j.xpro.2021.100928

SUMMARY

Tracking individual cell movement during development is challenging, particularly in tissues subjected to major remodeling. Currently, most live imaging techniques in *Xenopus* are limited to tissue explants and/or to superficial cells. We describe here a protocol to track immature multiciliated cells (MCCs) moving within the inner epidermal layer of a whole embryo. In addition, we present a data processing protocol to uncouple the movements of individual cells from the coplanar drifts of the tissue in which they are embedded.

For complete details on the use and execution of this protocol, please refer to Chuyen et al. (2021).

BEFORE YOU BEGIN

This protocol provides a comprehensive and detailed description of live imaging techniques aimed at tracking individual cell movements *in vivo* during *Xenopus laevis* embryonic development. The essential materials are *X. laevis* embryos, spinning-disk confocal microscope, the commercial software Metamorph, the open source software Fiji (ImageJ) and Python scripts. Cells are fluorescently labelled in living *X. laevis* embryos by standard microinjection of plasmid DNA and mRNA. In the present case, where MultiCiliated Cells (MCCs) are tracked, the expression of green fluorescent proteins in free form or fused to other proteins or peptides, such as LifeAct, is under the control of the MCC-specific α-tub promoter (Stubbs et al., 2006). To this aim, 8- to 16-cell-stage *Xenopus* embryos are injected as described below.

KEY RESOURCES TABLE

REAGENT or RESOURCE	SOURCE	IDENTIFIER
Chemicals, peptides, and recombinant proteins		
UltraPure™ Low melting point Agarose	Invitrogen™	16520–050
Mineral oil		
Benzocaine		
Ficoll™ PM 400 (Dry Powder)	Cytiva™	17030050
Recombinant DNA		
pαtub::GFP	Stubbs et al. (2006)	N/A
pCS2+mRFP	Stubbs et al. (2006)	N/A
pαtub::LifeActGFP	Chuyen et al. (2021)	N/A
Experimental models		
X. laevis (wild-type)	NASCO (https://www.enasco.com)	N/A

(Continued on next page)

Continued

REAGENT or RESOURCE	SOURCE	IDENTIFIER
Software and algorithms		
FIJI-Image J	https://imagej.net/Fiji	N/A
Image Stabilization home-made scripts	Chuyen et al. (2021)	https://github.com/fabda/mcc_paper

MATERIALS AND EQUIPMENT

1× Modified Barth's Saline

Reagent	Final concentration	Amount
NaCl	88 mM	
KCl	1 mM	
$NaHCO_3$	2.4 mM	
$MgSO_4$	0.82 mM	
$Ca(NO_3)_2$	0.33 mM	
$CaCl_2$	0.41 mM	
HEPES	10 mM	
NaOH	Adjust pH to 7.4	N/A
ddH_2O	n/a	Up to 1 L

Adjust pH to 7.4 with 10 M NaOH. After sterilization by autoclaving, store at room temperature (20°C–25°C).

Embedding culture medium

Reagent	Final concentration	Amount
LMP Agar	0.8 g/L	0.8 g
Pharmacological inhibitor (optional)	N/A	N/A
0.1× MBS	0.1×	1 L

Store at room temperature (20°C–25°C) or at −20°C when pharmacological inhibitor is included. Melted at 37°C in water bath before embedding.

STEP-BY-STEP METHOD DETAILS
Step 1: Expression of fluorescent proteins in *xenopus* embryos

⏱ Timing: 3–4 days

The protocol is adapted from Early Development of *Xenopus laevis*: A Laboratory Manual (Sive et al., 2000) and Obtaining *Xenopus laevis* embryos (Shaidani et al., 2021).

1. To obtain *X. laevis* eggs, stimulate ovulation in *X. laevis* adult females by subcutaneous injection of (800 units/animal) Human Chorionic Gonadotropin (Chorulon[R]) into the dorsal lymph sacs.
2. From 16 to 24 h post-stimulation, collect eggs from stimulated females by manual squeezing. Eggs are collected in empty Petri dishes.

3. Perform *in vitro* fertilization with sperm from adult males.
   a. To collect sperm for *in vitro* fertilization, the males need to be euthanized to explant the testes. Males are euthanized by immersion in a 2 liter bath of benzocaine solution (2,6 mL/L) through immersion of frogs in benzocaine bath (2 liter per frog) for 15 min followed by cervical sectioning of the spinal cord posterior to the skull.

   Note: Before cervical sectioning, check that the male is unresponsive to foot pinching with tweezers.

Using dissection scissors, cut through the skin and the abdominal muscles to open the lower abdominal cavity on the ventral side.

The testes are found on the dorsal side of the cavity, on either side of the aorta, behind the fat bodies.

Cut the testes out and trim away any attached fat and viscera.

Transfer at 4°C in 0.1× MBS (Modified Barth's Saline; see the recipe for 1× MBS below) for *in vitro* fertilization on the same day.

Note: testes can be stored at 4°C in Leibovitz's L-15 Medium, GlutaMAX™ Supplement culture media (ThermoFisher) for up to a week without significant loss of sperm viability.

b. Cut a quarter to a third of testis and crush it with a plastic microcentrifuge pestle in 0.5 mL of 0.1× MBS into a 1.5 mL microcentrifuge tube.

c. With a glass pipet, deposit the solution of crushed testis evenly on the eggs. Use the plastic pestle to distribute the eggs into a monolayer on the Petri dish and wait for 5 min before covering them with 0.1× MBS for 1.5 h.

4. De-jelly the fertilized eggs with gentle agitation for about 10 min in 2% cysteine in 0.1× MBS at pH 8. The cysteine solution should be prepared immediately before use. Once the jelly-coat is dissolved and the eggs have started to pack, wash extensively in water to remove the cysteine. Note: Prolonged exposure to cysteine will damage embryos.

5. Keep embryos in 0.1× MBS at 13°C, 18°C or 23°C until they reach the stage suitable for injection (8- or 16-cell).

6. Once the first cell division is completed, transfer embryos in Ficoll 4% in 1× MBS

7. Prepare materials for microinjection:

a. Micro-manipulation and micro-injection device Nanoject II (Drummond).

b. Pull glass needles from 1.14 mm (outer diameter) × 3.5" length × .53 mm (inner diameter) glass microcapillaries (3.5" Drummond #3-000-203-G/X) with a needle puller (inner tip diameter must be 10–30 μm).

c. Back-fill the glass needle with mineral oil using a Drummond syringe with a 30 gauge, 2" long blunt needle, (Drummond Scientific). Pay special attention to avoiding air bubbles. Mount the glass needle on a micro-manipulator. Break the tip of the glass needle with surgical grade tweezers, at an angle of 45°.

d. Short before injection, prepare the injection mix (Table 1) with mRNA coding for mRFP (500 pg/blastomere) and pα-tub::GFP or pα-tub::LifeActGFP (50–60 pg/ blastomere). Both plasmids must have been previously linearized by NotI.

Note: Plasmid linearization increases the number of GFP-positive MCCs.

e. (Optional) Constructs can be co-injected with morpholinos to deplete specific proteins. **Note**: Morphant cells can be visualized by mRFP tracer co-injected with morpholinos. Alternatively, fluorescent morpholinos can be used to directly visualize live morphant MCCs.

Table 1. Constructs used in microinjection

Construct name	Injection amount (final concentration in the injection mixture)	Function
pα-tub::GFP or pα-tub:: LifeActGFP	6 pg/nl or 3 pg/nl	Labels MCC cell body or MCC actin cytoskeleton
mRFP mRNA	50 pg/nl or 25 pg/nl	Injection tracer. Importantly, mRFP labels outer layer cell membranes, which is required for image stabilization post-acquisition

Note: adjust the concentration of each construct to the final volume to be injected in each blastomere: injection volume per blastomere of 10nl is preferentially used but it can be increased to 20nl when injection mixture includes morpholinos.

    f. Deposit a 1–3 μL drop of the injection mix on the bottom of a plastic Petri dish and load it into the glass needle by suction.

8. Inject the loaded construct mix under the apical surface of the ventral animal blastomeres (precursors of the non-neural ectoderm) of 8 cell- or 16 cell-stage embryos. Ventral blastomeres can be distinguished by their darker pigmentation

    Note: to maximize the number of fluorescent MCCs, both ventral animal blastomeres of 8 cell-stage embryos are injected. On the other hand, mosaicism can be increased by injecting only two of the four ventral animal blastomeres of 16 cell-stage embryos.

9. Transfer embryos in 2% Ficoll in 0.1× MBS and culture at 13°C.
10. Culture embryos in 0.1× MBS for 1–2 days at the preferred temperature (13°C–23°C) until the first signs of stage 14 (earliest stage at which α-tub-driven expression of fluorescent proteins can be detected in the injected MCCs; see developmental table).

    Note: Incubation of sibling injected embryos at different temperatures will result in different developmental rates (Nieuwkoop et al., 1994), thus allowing to perform several live imaging experiments with a single batch of injected embryos. For example, embryos cultured at 23°C are ready for imaging 15 h post-injection while embryos cultured at 13°C can be imaged 48 h post-injection.

    Note: Considering the possibility of sample loss caused by embryo death or embedding problems, we recommend to inject at least 10–15 embryos per condition.

11. (Optional) Pharmacological inhibitors can be added to the culture medium. In Chuyen et al. (2021), Axitinib or CK-666 was added to culture medium from stage 12 onwards.

Step 2: Preparation of sample for live imaging

  ⏱ Timing: 30 min

Immobilization of samples is the key step for successful live imaging (Bostock et al., 2020). The α-tub-driven expression of fluorescent reporter proteins in MCCs becomes detectable around stage 14 (25 h post fertilization at 18°C) but in the following hours the embryonic epidermis is subjected to significant strains due to embryo elongation, which can affect the process of image acquisition. The method we propose here is a home-made montage to limit tissue movement during live imaging. A list of possibly encountered problems has been established (see problems 1 and 2 in Troubleshooting).

12. As soon as embryos reach stage 14, sort the fluorescently labeled embryos under a stereomicroscope (excitation/emission settings for GFP (488/510) and RFP (532/588)).

    Note: Due to the mosaicism caused by unequal plasmid inheritance, not all MCCs may be labeled and fluorescence intensity may increase with time, leading to the detection of additional MCCs during recording. By default, select embryos with the highest number of GFP-positive MCCs.

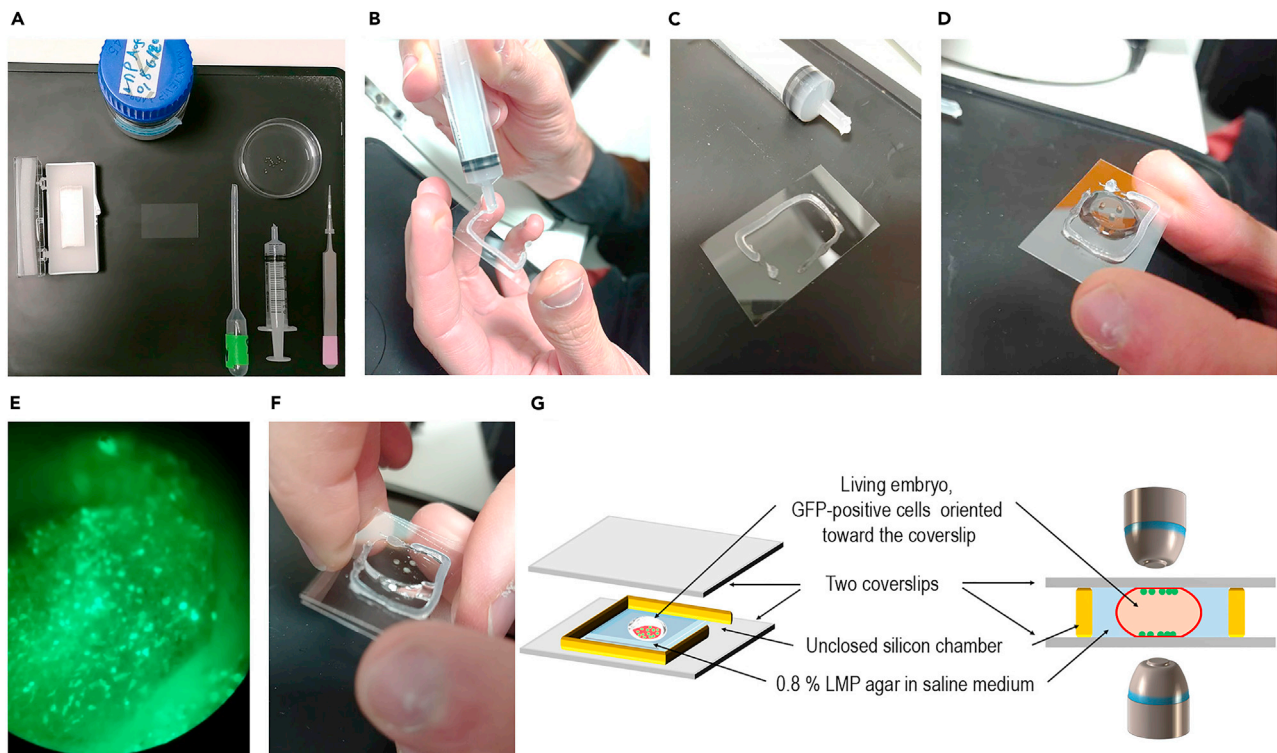13. Prepare the embedding medium (Figure 1)

Figure 1. Embedding of embryos for live imaging

(A) Equipment and materials required for experiment: 100 mL glass bottle containing molten 0,8% low melting point agar in 0,1× MBS; box of 24*40 mm coverslips; a petri dish containing transfected stage 14 embryos with MCCs expressing fluorescent reporter; plastic pipette or flame-polished glass Pasteur pipette, needle-less syringe filled with silicon grease and forceps.

(B) Using a 10 mL needle-less syringe filled with silicon grease, delimit a roughly 2cm² area chamber onto a 24*40 mm coverslip but do not completely close the chamber.

(C) Image of a 2cm² open silicon chamber onto a 24*40 mm coverslip.

(D) Silicon chamber filled with 3–4 drop of molten agar and 4 embryos.

(E) Image of an embryo with field of GFP-positive cells oriented upward.

(F) Embedded embryos between two coverslips ready for live imaging.

(G) Schematic illustration of embryo embedding between two coverslips. Right panels represent transversal view of flatten embedded embryo, which can be imaged from both sides.

    a. With microwave or 37°C water-bath, melt 0.8% low melting point (LMP) Agar in 0.1× MBS.

Note: when melted with microwave, wait until the solution goes below 40°C (roughly, when it becomes possible to hold the tube bare-handed).

    b. (Optional) If embryos have been treated with a pharmacological inhibitor and if the treatment must be extended during time-lapse recording, the inhibitor can be added to molten LMP Agar

Note: in this case, melt with 37°C water-bath to avoid thermal destruction of the inhibitor

    c. Using a 10 mL needle-less syringe filled with silicon grease, delineate a chamber of roughly 2cm² area onto a 24×40 mm coverslip (Figures 1B and 1C).
    d. Using a flame-polished glass Pasteur pipette or plastic pipette fill the chamber with 3–4 drops of molten agar (Figure 1D).

Note: keep the silicon chamber opened to allow air exit when the second coverslip is applied (Figure 1C).

14. Using a flame-polished glass Pasteur pipette or plastic pipette, drop 4–5 selected embryos in molten agar (Figure 1D) and position them with the help of a forceps, such that the regions richest in GFP-positive MCCs face upwards (this can be done under a fluorescent dissecting microscope) (Figure 1E).

    Note: the time between steps 2 and 3 should not exceed 2minutes to prevent the agar from hardening (see troubleshooting 1)

15. Quickly seal the silicon grease chamber with a second coverslip before the agar sets (Figure 1F).

    Note: embryos might roll during the sealing process. If this happens, it is possible to rotate them back in a favorable position by gently sliding the two coverslips against each other. If embryos have entirely rolled over and GFP-positive MCCs locate on the other side, this technique increase by two-fold the chance of success of getting an optimal field for live imaging since cells may be filmed through the bottom coverslip (Figure 1G).

16. Press gently the two coverslips to slightly flatten the embryos without crushing them (Figure 1G).

    ⚠ CRITICAL: since developmental stage cannot be estimated once embryos are embedded we recommend to start live imaging experiment immediately after embedding.

Step 3: Spinning-disk confocal live imaging of MCCs in embryonic epidermis

   ⏱ Timing: 2–8 h

MCCs start expressing fluorescent reporters when they are still irregularly distributed within the inner layer of the epidermis. During image acquisition, MCCs first migrate within the plane of the inner layer to disperse at regular intervals and later migrate radially to intercalate among outer-layer cells. To record the movements of MCCs through the thickness of the two epidermal layers, we use spinning-disk confocal microscopy to acquire z-stack images at high speed. Our protocol was designed to characterize MCC movements relative to each other and to outer-layer cell junctions. We also wanted to measure the time of contact between MCCs, the evolution of MCC speed relative to mutual contact events and the MCC migration path relative to outer-layer cell junctions.

Thus, it is critical to choose samples in which MCC labeling and orientation are optimal. Since MCCs randomly migrate laterally, some MCCs may exit the region of interest, while others may enter it. For the successful exploitation of time-lapse movies, it is essential to maintain the same field of view via frequent manual realignment.

   Note: As the embryo has a convex surface, the ideal region to be filmed is where the epidermis is flattened by contact with the coverslip.

17. Position the coverslip 'sandwich' in the imaging chamber of the Nikon Roper spinning-disk Eclipse Ti inverted confocal microscope.

    Note: the chamber must be stabilized at 23°C to reduce developmental variability between experiments.

18. Choose the objective and select the optimal field with mercury lamp HBO 50 W fluorescent illumination.
19. Set up microscope for z-stack time-lapse acquisition: 20μm-deep Z sections; z-step = 0.5–0.7 μm; 2 frames averaging; time interval 30 s–2 min (depending on the number of channels used).

20. Adjust exposure time and laser power to the fluorescence intensity of the different channels.

    Note: the z stack acquisition time must be at least 5–10 sec shorter than the time interval between stacks (see step 12).

21. Select a field of interest and set your stacks range taking as reference the 561 nm channel and the surface of the outer layer cells for the most apical z and the 491 nm channel, which labels the MCCs within the inner layer for the most basal z.
22. Launch time-lapse acquisition for 2–10 h. Note: Although some fluorescent cellular debris can be observed (Icha et al., 2017) the use of a fluorescent caspase activity reporter never revealed significant cell death (Chuyen et al., 2021). However, tissue collapse has been reported in experiments which last longer than 10 h .
23. During embryo development, morphogenetic movements will cause displacements in X, Y or Z direction. Whenever necessary, adjust manually the X, Y and Z axes, taking advantage of the 5–10sec lapse of time between stacks using the joystick Nikon TI-S-EJOY system (see point 3 in troubleshooting).

Step 4: Movie stabilization and quantitative analysis of MCC behavior

⏱ Timing: 1 day

Raw data obtained with spinning-disk confocal time-lapse imaging are processed for image and movie visualization and further quantification as indicated below. The multidimensional images are processed with the imageJ/Fiji free software and two individual homemade Python scripts.

24. Z-stacks from confocal video microscopy are converted into single plane projection by maximum intensity or sum intensity projection. Each channel is processed separately with the optimized z-section corresponding to the outer/inner layer cell staining.

25. Stabilization of movements caused by tissue growth in the x,y axis is done as following:
    a. With "manual tracking "Fiji plugin (https://imagej.net/plugins/manual-tracking), a single vertex is tracked frame by frame to extract its coordinates as reference for movie stabilization.
    b. A first Python 3 script has been developed to quantify this latter tracked vertex drift at frame level and correct it (see https://github.com/fabda/mcc_paper/refocus.py).
    c. We then use the "Image Stabilizer" Fiji plugin (https://imagej.net/Image_Stabilizer), which implements the Lucas-Kanade algorithm to further stabilize the movie (Figure 2 and Methods video S1).

    Note: Depending on the filmed region, embryo morphogenetic movements can cause heterogeneous tissue deformation, which complicates image stabilization. This is particularly sensitive with 10× or 20× magnification (see problem 4 in Troubleshooting).

26. Quantification of MCC migratory behavior:
    a. Stabilized movies are used to track all visible GFP-positive MCCs. The centroid of each cell is manually tracked with "manual tracking" Fiji plugin throughout each movie to analyze the migratory behavior of MCCs. Open the stabilized movie and create one track per MCC. One by one, click manually on the centroid of each MCC from the beginning to the end.

    Note: Finding position of MCCs can be difficult (see point 5 in troubleshooting).

    b. Another Python 3 script has been developed to generate a set of "behavioral descriptors" using the tracked MCC centroid file to further characterize the migratory behavior of MCCs: distance of displacement, cumulative travelled distance, migration direction, instant
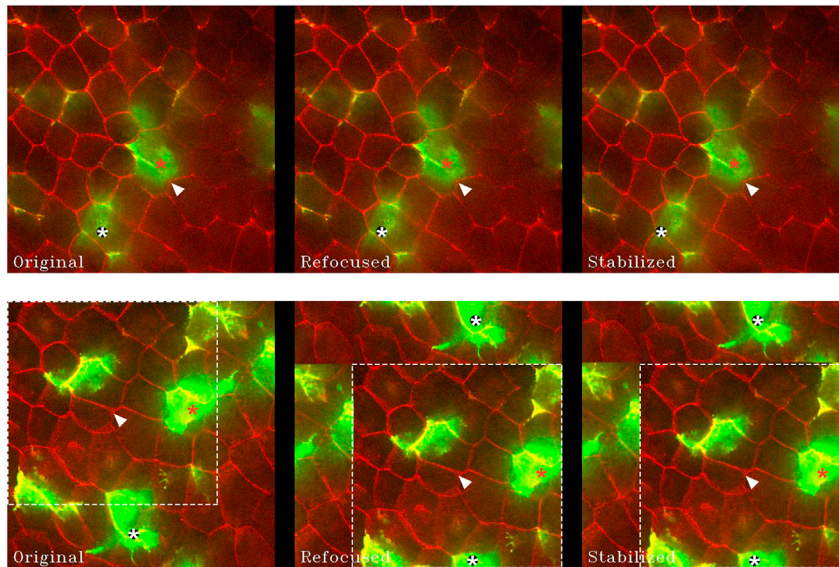
Figure 2. Illustration of a movie before and after the different steps of stabilization
Initial time point (top) and final time point (bottom) from projection of time-lapse movies (Methods video S1) are shown in original, refocused and stabilized format (refer to Quantification and Statistical Analysis, step 1 to 2). In the original movie, a reference vertex (white arrowhead) is tracked frame by frame through the movie. Using extracted coordinate of the tracked vertex, images are refocused to preserve the original position of that vertex. Next, stabilized images are obtained by using the "Image Stabilizer" Fiji plugin, which implements the Lucas-Kanade algorithm to further stabilize the movie. On the bottom images, the dotted squares demarcate the conserved frame with stabilized position. In the original movie, the tracked vertex has drifted from its initial position. In refocused and stabilized movies, the frame of interest is repositioned to maintain the tracked vertex on its initial position. Note that in refocused and stabilized movies, the MCC tracked in white has been cut by the reframing. Consequently, after reframing only MCCs within the conserved frame can be scored.

velocity. (see: https://github.com/fabda/mcc_paper/analysis.py). This script is fully parameterizable by the user: smoothing of centroid position (x,y) to avoid manual tracking artifacts (sigma parameter), smoothing of stabilization throughout the whole movie (window parameter), unit of measure relationship (pixmicron parameter), unit of time relationship (framesec parameter). An excel file is then generated containing all the "behavioral descriptors" for the given movie.

EXPECTED OUTCOMES

MCC spacing pattern in *X. laevis* had been addressed in several studies but live description of cellular behavior was missing (Deblandre et al., 1999; Stubbs et al., 2006). Over the past decade, radial intercalation of MCCs into the outer layer of the epidermis has been documented by video-microscopy (Chung et al., 2014; Szabó et al., 2016; Sedzinski et al., 2016, 2017; Kulkarni et al., 2018). However, cell movements within the plane of the epidermis have only been recently analyzed in live embryos (Chuyen et al., 2021; Collins et al., 2021). Using this protocol, MCCs can be observed in live *X. laevis* by spinning-disk fluorescent confocal microscopy (Figure 3A, Methods video S2). In addition, actin cytoskeleton dynamics can be monitored by expressing actin binding fluorescent peptides such as LifeAct::GFP (Figure 3B, Methods video S3), or actin nucleation promoting factors of the Arp2/3 complex, such as eGFP-p41 (Figure 3C, Methods video S4).

The generation of a regular distribution pattern of MCCs within the embryonic epidermis takes place between embryonic stages 14 and 25 in a time window of 10 h at 23°C. The regular spacing of MCCs relies on two concomitant phenomena: mutual repulsion among migrating MCCs and their affinity
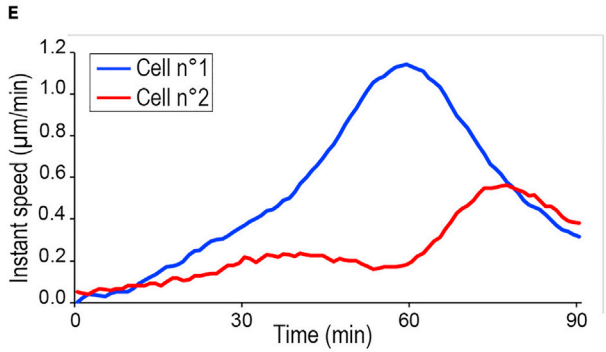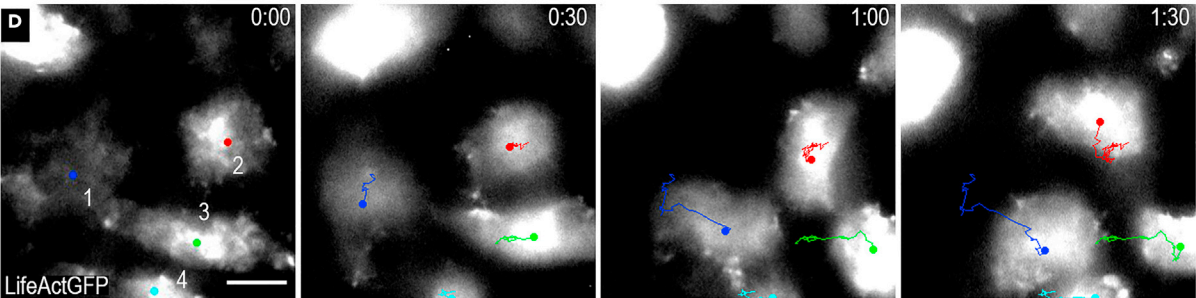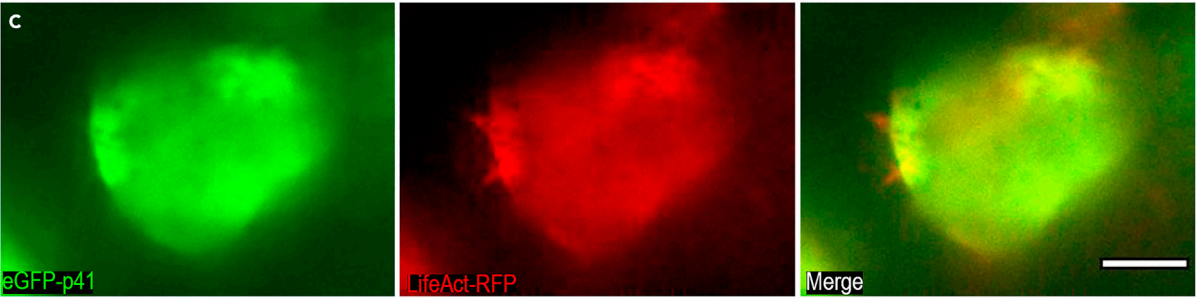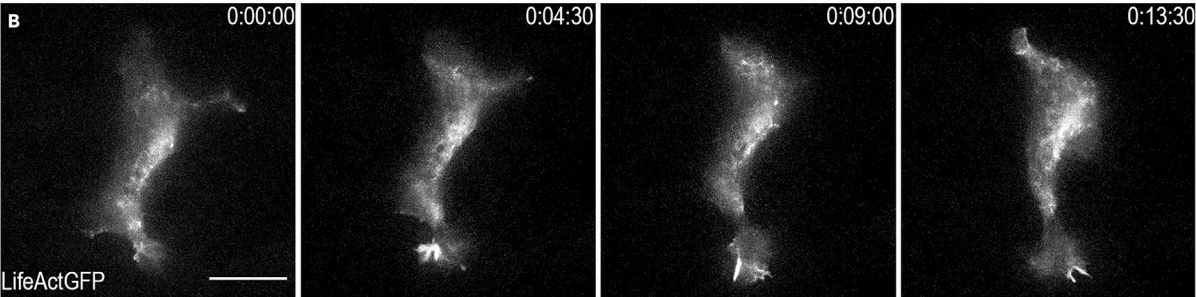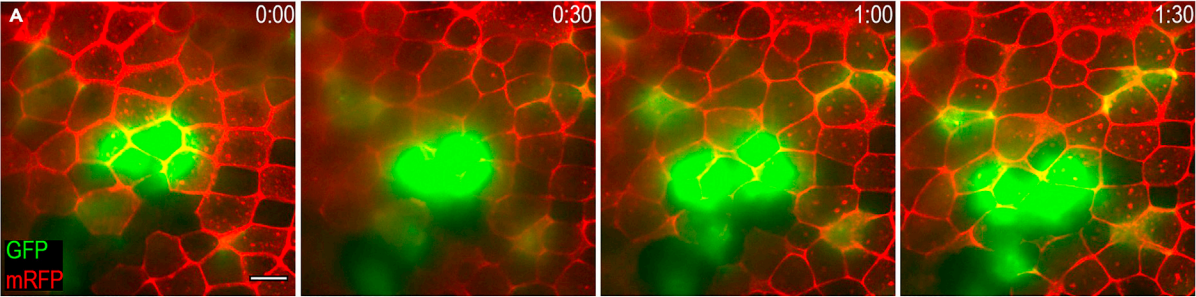
Figure 3. Live imaging of multiciliated cells in *Xenopus* embryonic epidermis

(A) Frames from unstabilized Methods Video S2 showing GFP-labelled MCCs within the epidermal inner layer and mFRP-labelled outer-layer cell junctions. MCCs shows irregular intensity of GFP-labelling, which is due to mosaicism caused by unequal plasmid inheritance. In the field, not all MCCs are labeled and fluorescence intensity increase with time, leading to the detection of additional MCCs during recording. Scale bar is 25 μm.

(B) Frames from Methods video S3 showing dynamic actin remodeling of a LifeActGFP-labelled MCC with generation of lamellipodia/filopodia protrusions. Scale bar is 15μm.

(C) Live signal of a single MCC from Methods video S4 showing the generation of LifeActGFP-labeled actin rich protrusions stimulated by local enrichment of Arp2/3 actin nucleation factor labelled with eGFP-p41. Scale bar is 15 μm.

(D) Frames from stabilized Methods video S5 showing tracked LifeActGFP-positive MCCs dispersing within the inner layer by mutual repulsion. Color dots represent the instant centroid of 4 tracked MCCs and the lines shows the migration path of these MCCs. Events of contact among MCCs are correlated with change in the direction of migration of colliding MCCs and evolution in their instant speed. Scale bar is 25 μm.

(E) Graph showing instant speed of MCC n°1 (dark blue) and MCC n°2 (red). After one hour, as MCC n°1 entered in collision with MCC n°3 (green) and MCC n°4 (light blue) its instant speed decreased. At the same time, MCC n°2 separated from MCC n°3 and its instant speed increased.

for outer-layer cell junctions, which constrains their motility and favors their positioning at vertices (junctions between 3 or more outer-layer cells), where they intercalate.

For most MCCs, these two phenomena can be detected within the first 3–5 h of recording. The lateral motility of MCCs then significantly decreases and is replaced by apical motility and radial intercalation for the last 5 h of the process. In Chuyen et al. (2021) time-lapse imaging was focused on the first phase prior to radial intercalation. The movement of MCCs was manually tracked on stabilized movies and evolution in cell speed was correlated to MCC mutual contact events (Figures 3D and 3E, Methods video S5).

> *Note:* Although we did not design this protocol to analyze radial intercalation, it is in principle applicable to this aim, which would require stabilization of all individual frames and orthogonal projection of the movie.

LIMITATIONS

Limitation 1

Impossibility to record MCC behavior at early developmental stages.

The live imaging protocol presented here provides detailed information on the dynamic behavior of MCCs within the inner layer and their lateral migration before the cells initiate radial intercalation into the outer layer. While data published in Chuyen et al. (2021) revealed that immature MCCs display migratory properties by stage 14, it is known that MCCs become fated at stage 11 (Deblandre et al., 1999), several hours before α-tub-mediated live imaging can be applied. Thus, the earliest phase of MCC behavior currently remains out of reach with our protocol, although this may change with the future characterization of earlier-active MCC-specific promoters.

Although our method was only applied to MCCs, other cell types populate the inner layer of the epidermis, such as ionocytes and small secretory cells. We speculate that the protocol presented here will be applicable to characterize their behavior after generation of constructs able to drive expression of fluorescent reporters in immature ionocytes (Stubbs et al., 2006; Quigley et al., 2011), small secretory cells (Dubaissi et al., 2014) or basal cells (Haas et al., 2019).

Limitation 2

Impossibility to record MCC behavior over more than eight hours.

In Chuyen et al. (2021), live imaging usually lasted 3–5 h. When attempting to record for more than 10 h, the integrity of embryos was lost, making it impossible to film the entire sequence of events from the initial spacing of MCCs up until their emergence at the surface of the epidermis. It is possible that the low melting point agar required to limit tissue movement during image acquisition eventually prevents proper embryo morphogenesis and/or survival. In unpublished data, we have

been able to track MCCs during radial intercalation, but we foresee that the same limitations for long-term imaging may apply and may be aggravated by the acquisition of muscle contractility later in development.

TROUBLESHOOTING

Problem 1

Embryo embedding problems (related to step 2)

Possible problems may arise during embryo embedding:

Embryos are deformed when the silicon chamber is sealed by the second coverslip

Embryos exit the silicon chamber when the coverslip is applied

Embryos are crushed when the second coverslip is applied

The second coverslip does not stick to the first one

Potential solution

Several reasons can non-exclusively explain embedding issues

The agar hardens too fast:

The time from agar deposition to chamber sealing should not exceed two minutes, to avoid the agar from hardening and deforming embryos or even crushing them. It often happens that the time needed to orient embryos is too long and the agar starts to harden, resulting in the deformation of embryos when the top coverslip is applied. We recommend mounting a maximum of 5 embryos, which allows enough time to optimize orientation before the agar hardens.

Too much liquid is poured in the silicon chamber:

If the volume of molten agar plus the culture medium containing the embryos exceeds the chamber capacity, the application of the top coverslip will chase away the excess liquid and the embryos might be carried away with the flow. We recommend not to exceed 4 drops of molten agar and adding as little liquid as possible when embryos are deposited. It is also important that the chamber is not completely sealed otherwise air bubbles might chase away the liquid and embryos. Moreover, liquid covering the silicon grease may prevent adherence to the coverslip.

The molten agar is too warm:

Hot agar will affect embryo integrity, which will become less resistant to embedding

The amount of silicon is not adapted:

If too much silicon grease is deposited on the coverslip, the capacity of the chamber may be reduced and may cause it to close, which would prevent expulsion of air bubbles. On the contrary, if not enough silicon is applied, the two coverslips may not properly stick to each other and embryos may be crushed during mounting.

Problem 2

Difficulty to expose the region of interest during embryo embedding (related to step 2)
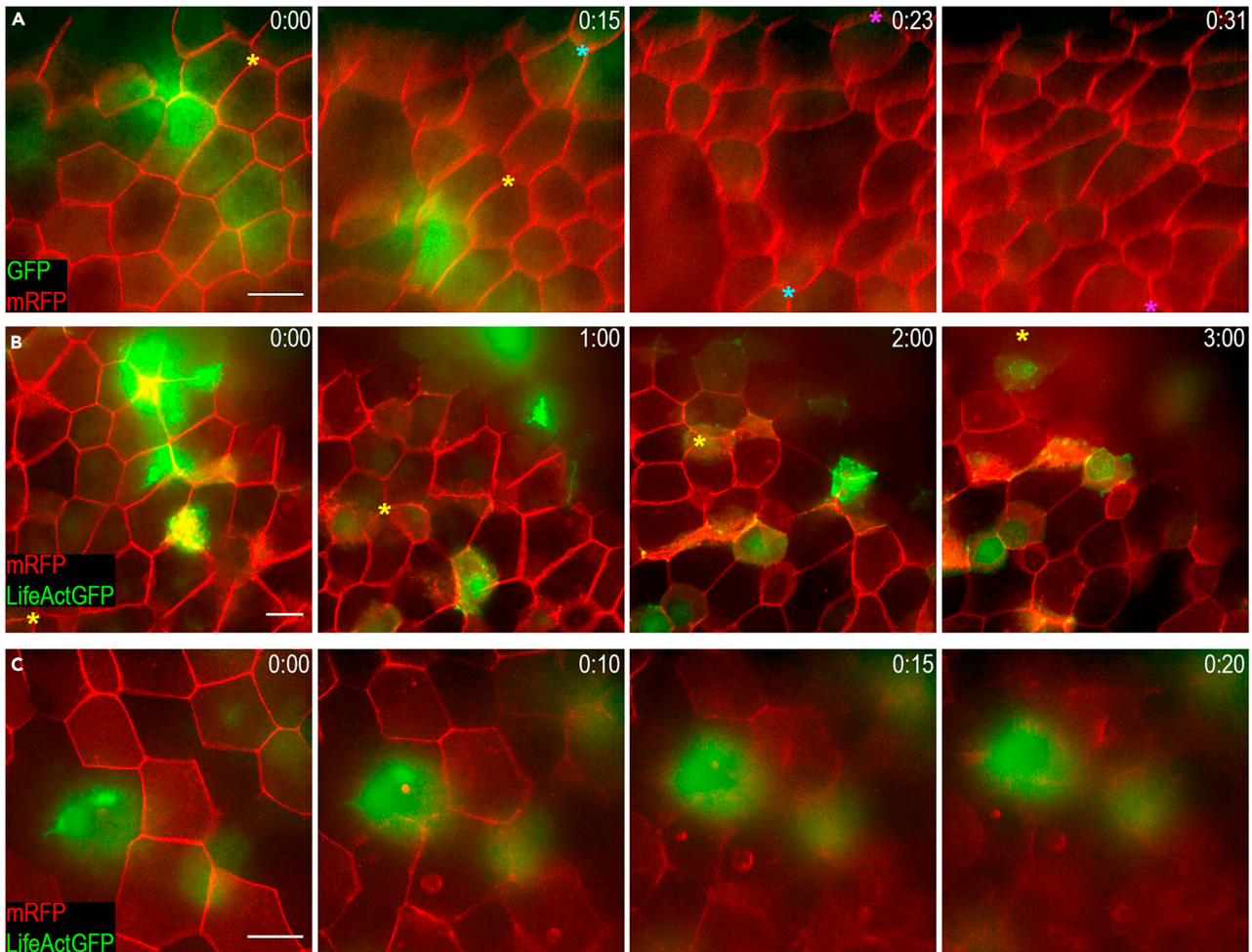
Figure 4. Examples of excessive drift where stopping image acquisition is preferable because it may result in non-exploitable data

(A) Frames from Methods video S6 showing excessive x,y drift. Several vertices are tracked with color asterisks showing that between time t and t+1, each tracked vertex completely crosses the recorded field.

(B) Frames from Methods video S7 with a selected zone of interest on the border of the flattened region of the embryo. The yellow asterisk shows a single tracked vertex illustrating the significant tissue drift and the loss of information in the upper right corner due to embryo curvature.

(C) Frames from Methods video S8 illustrating the rapid loss of focus caused by excessive z drift.

In all cases, scale bar is 25 μm.

With our embedding method, it is not possible to precisely orient the sample, such that GFP-positive MCCs can be optimally exposed to be filmed.

Potential solution

To limit this risk, we recommend injecting over 15 embryos per condition.

Problem 3

x, y or z drift during image acquisition (related to step 3)

A major aim of this protocol is to give insights about sample immobilization during image acquisition through embedding (steps 2–5). We develop here potential solutions to limit drift in x, y and z positions and scenarios in which it is preferable to stop image acquisition because excessive drift may result in non-exploitable data (Figure 4, Methods videos S6, S7, and S8).

Potential solution

Wisely choose the region of interest

Embedding results in flattening of the epidermis in contact with the coverslips (Figure 1G, right panel). We do not recommend selecting a zone of interest on the border of the flattened region as the drift might increase as the embryo grows. We instead recommend selecting a zone of interest in the center of the flattened region where the drift in x,y axis is lower and where outer-layer cell junctions are on the same z plane, making it easier to maintain the focus.

Check the evolution of the movie and adjust manually in x, y and z:

As image acquisition takes place on the Metamorph software, images will be automatically saved. In parallel to image acquisition, open the saved images with FIJI/ImageJ software to visualize and annotate the evolution of the sample over time (Figure 5). Use the arrow tool to track the position of a reference point in outer layer cell junction at time 0 (a given vertex can be an ideal reference). Measure in which direction the vertex moves in the x and y axis to estimate the direction of the drift and its severity. Then during the 10 s lap between two z series acquisition, use the control joystick to manually adjust the position of the frame so as to place the reference vertex back on its initial position, allowing to track the same frame over time. For z adjustment, play the movie at a given and easy to recognize z plane (apical surface for example). Any change on the observed plane will indicate a drift in z axis, in which case adjustment in z must be done manually, similar to x/y adjustment.

> *Note:* manual adjustments are required every 5–20 minutes (depending on the drift amplitude).

> *Note:* since the drift can change direction through time, frequent manual adjustment can be required. The more often manual adjustment is done the better the movie quality will be.

> *Note:* Avoid adjusting during z series acquisition to prevent artifactual blurring.

In silico stabilization of movies:

The image processing method presented above will easily deal with minor drifts in x and y axes, as long as the focus in z axis allows visualizing the outer-layer cell junctions. Be aware, however, that reframing will inevitably cause cropping around the initial region of interest, and loss of information outside that region (Figure 2).

Problem 4

Heterogeneous tissue remodeling complicates image stabilization (related to step 4)

Our protocol easily allows for image stabilization in tissues undergoing homogeneous deformation, but its efficiency may decrease as heterogeneities in tissue deformation emerge. Obviously, the perception of heterogeneous deformation is scale-dependent and more severe when movies are taken at lower magnification. Our protocol was initially designed for 40–60× magnification experiments aimed at tracking few interacting MCCs (Figures 6A and 6B, Methods video S9). However, filming at lower magnification can be useful, as this increases the number of cells visible per field and thus allows a faster and more representative quantification of the phenomenon (Figures 6C and 6D, Methods video S10). In our stabilization protocol, vertices from outer layer junctions serve as physical reference to identify and correct the drift (Figures 6A'–6D'). At 40× magnification, the image stabilization significantly reduces the drift (Figures 6A, 6B, 6A', 6B', and 6F, Methods video S9) (Chuyen et al., 2021). However, this may not be sufficient at 20× magnification, as the tissue
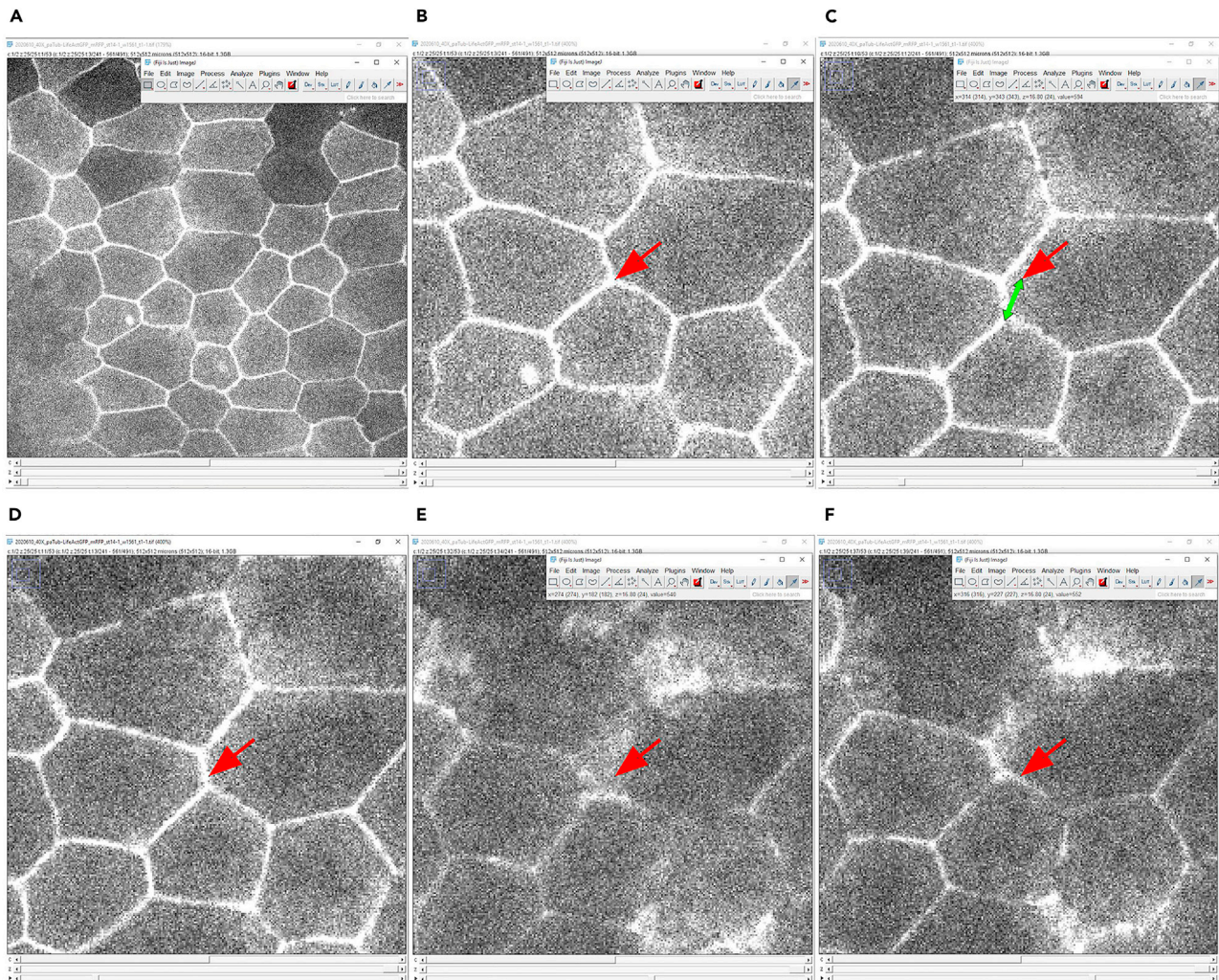
Figure 5. Examples of manual adjustment in drifting sample during image acquisition

(A) Import the sequential images into Fiji (ImageJ) as hyperstacks from ongoing live imaging experiment. Position the hyperstacks on the channel 1, which corresponds to outer-layer cells labeled with mRFP at time point 1 (initial time point) and z 25/25 (the top z on the series).

(B) Zoom on image and select a vertex, which will be used as a reference to correct x,y drift over time. Draw an arrow with the arrow tool on this vertex. The arrow will remain in constant position, while the vertex will change position if the tissue drifts.

(C) Green double arrowhead illustrates the drift in x and y axes after 9 min of acquisition. To optimize exploitation of the ongoing experiment the drift should be corrected.

(D) Illustration of x and y manual adjustment during the time pause between two z-series. The experimenter has used the control joystick to reposition the tracked vertex to its initial position based on the estimated x,y drift.

(E) Twenty minutes later, the z drift has caused the signal of outer-layer junctions on the most apical recorded z to not correspond to the surface of the sample.

(F) Illustration of z axis manual adjustment during the time pause between two z-series. The experimenter has used the control joystick to reposition the top z to the surface of the sample.

is exposed to heterogeneous remodelling (Figures 6C, 6D, 6C', 6D', and 6 F, Methods video S10). Indeed, the quality of image stabilization varies relative to the distance from the vertex used as reference: regions closer to the reference point will be properly stabilized (Figures 6C' and 6D', dark blue dot and line, Methods video S10), while the more distant ones are still drifting (Figures 6C' and 6D', light blue and red dots and lines). Thus, live-imaging at 20× magnification significantly increases the variability of the drift (Figure 6F) to an extent that may compromise the quantifications of MCC motility.
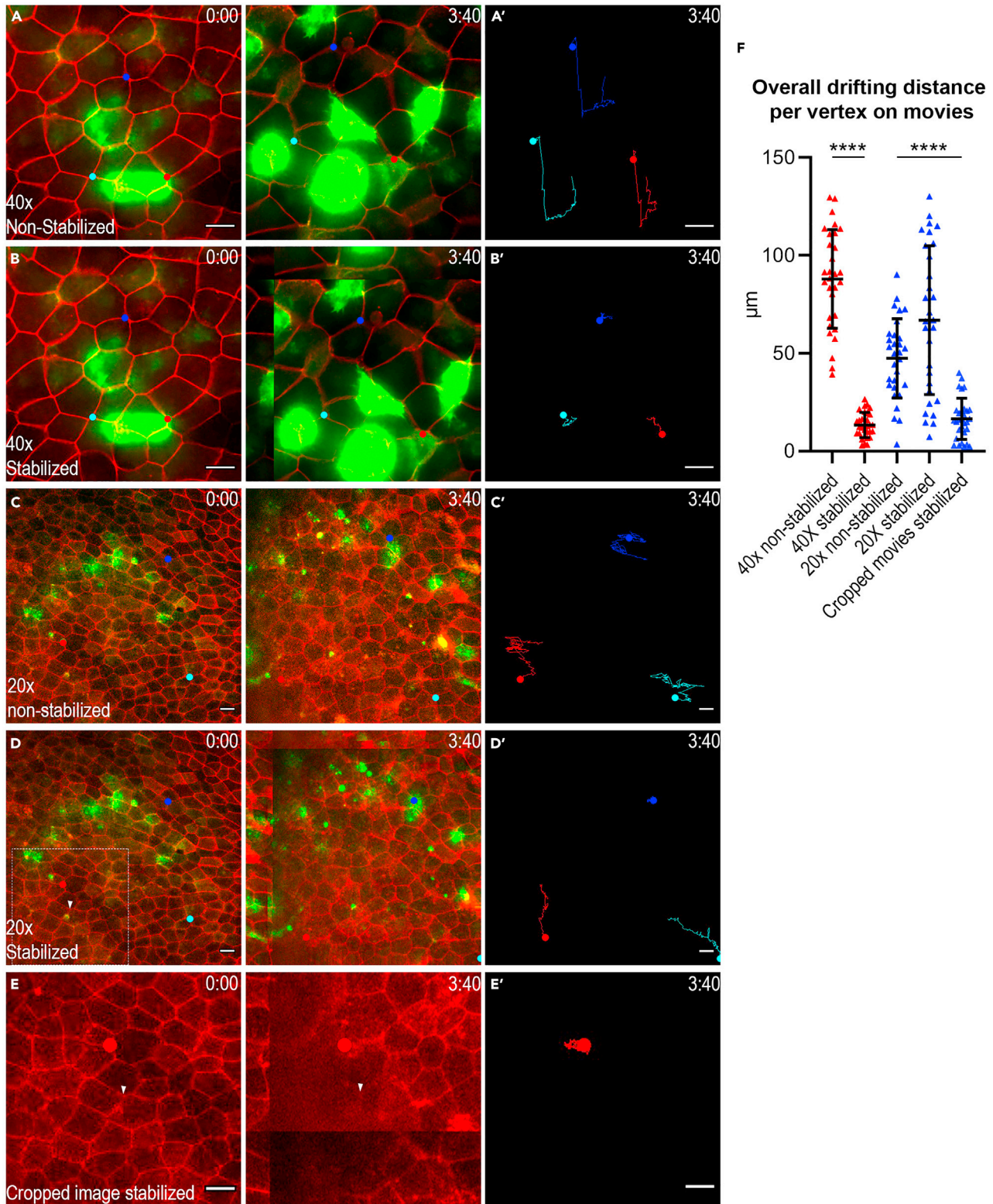
Figure 6. Image stabilization quality varies with magnification

(A–E) Still views of initial time point (left) and final time point (right) from time-lapse movies recorded at 40× (Methods videos S9A and S9B) or 20×
magnification (Methods videos S10A and S10B) before (A and C) and after stabilization (B and D). For each image, the red signal corresponds to outer-

Figure 6. Continued

layer cells labeled with mRFP and the green signal corresponds to MCCs expressing LifeActGFP. The drift between initial and final time points are illustrated with labeled vertices (light blue, dark blue and red). (E) Initial time point (left) and final time point (right) from a cropped section of the movie (Methods video S10C). The crop was extracted from the region boxed in Figure 6D and stabilized using the vertex shown with the white arrowhead as reference.

(A′–E′) Dots and lines in light blue, dark blue and red represent the drift of the corresponding tracked vertices over time in movies before (A′ and C′) or after stabilization (B′, D′, and E′). In stabilized movies (B′, D′, and E′) all vertices are not stabilized with the same efficiency, as a consequence of heterogeneity in cellular rearrangement.

(F) Dot plot showing the drift, as a distance between the position of vertices at initial and final time points. While image stabilization significantly decreases the drift of most vertices filmed at 40× magnification, the drift is incompletely corrected for vertices filmed at 20× magnification. The quality of the stabilization decreases with the distance to the reference vertex. The drift is significantly corrected in movies cropped to the size of a 40× magnification. For all images, the scale bar is 25 μm. **** is p-value <0.0001.

Potential solution

As shown in Figures 6A–6D and 6F, the quality of image stabilization significantly decreases with wider fields obtained with lower magnification. Since the intensity of the post-stabilization drift is proportional to the distance from the reference point, we recommend to crop the movie in smaller areas (e.g., white dotted square, Figure 6D) when the sample is facing heterogeneous drift, and independently stabilize each crop (Figures 6E and 6F). In each crop, a reference vertex central to the image may be used for movie stabilization (e.g., white arrowhead in Figures 6D and 6E). This approach shows significant improvement in reducing local drift compare to wider fields (Figure 6F). We recommend to carefully check stabilized movies to avoid counting artificial movements due to improper stabilization.

Problem 5

Difficulty to identify individual MCCs during cell tracking (related to step 4)

Because of mosaicism caused by plasmid injection, all MCCs are unequally labeled. Furthermore, new MCCs starting to express the plasmid later may emerge during image acquisition. High MCC density and signal heterogeneity are an issue when tracking individual MCCs at early stages.

Potential solution

When identification of MCCs at early stage is difficult, one solution is to reverse time on Fiji (Image > Stacks > Tools > reverse). This way individual cells which are easily identifiable at the end of movies will be easier to track.

RESOURCE AVAILABILITY

Lead contact

Further information and requests for resources and reagents should be directed to the lead contact, Laurent Kodjabachian (laurent.kodjabachian@univ-amu.fr).

Materials availability

Plasmids generated for this study are available from the lead contact.

Data and code availability

The codes written to analyze time-lapse movies are deposited in Github. (https://github.com/fabda/mcc_paper).

SUPPLEMENTAL INFORMATION

Supplemental information can be found online at https://doi.org/10.1016/j.xpro.2021.100928.

AUTHOR CONTRIBUTIONS

Conceptualization: A.C., A.P., and L.K. Methodology: A.C., F.D., and A.P. Software: F.D. Formal analysis: A.C. and F.D. Investigation: A.C. and F.D. Validation: A.C., F.D., A.P., and L.K. Resources: L.K. Supervision: A.P. and L.K. Project administration: A.P. and L.K. Funding acquisition: A.P. and L.K. Writing – original draft: A.C. Writing – review and editing: F.D., A.P., and L.K.

DECLARATION OF INTERESTS

The authors declare no competing interests.

REFERENCES

Bostock, M.P., Prasad, A.R., Chaouni, R., Yuen, A.C., Sousa-Nunes, R., Amoyel, M., and Fernandes, V.M. (2020). An immobilization technique for long-term time-lapse imaging of explanted Drosophila tissues. Front. Cell Dev. Biol. *8*, 590094. https://doi.org/10.3389/fcell.2020.590094.

Chung, M.-I., Kwon, T., Tu, F., Brooks, E.R., Gupta, R., Meyer, M., Baker, J.C., Marcotte, E.M., and Wallingford, J.B. (2014). Coordinated genomic control of ciliogenesis and cell movement by RFX2. eLife *3*, e01439. https://doi.org/10.7554/eLife.01439.

Chuyen, A., Rulquin, C., Daian, F., Thomé, V., Clément, R., Kodjabachian, L., and Pasini, A. (2021). The Scf/Kit pathway implements self-organized epithelial patterning. Dev. Cell *56*, 795–810.e7. https://doi.org/10.1016/j.devcel.2021.02.026.

Collins, C., Kim, S.K., Ventrella, R., Carruzzo, H.M., Wortman, J.C., Han, H., Suva, E.E., Mitchell, J.W., Yu, C.C., and Mitchell, B.J. (2021). Tubulin acetylation promotes penetrative capacity of cells undergoing radial intercalation. Cell Rep. *36*. https://doi.org/10.1016/j.celrep.2021.109556.

Deblandre, G.A., Wettstein, D.A., Koyano-Nakagawa, N., and Kintner, C. (1999). A two-step mechanism generates the spacing pattern of the ciliated cells in the skin of Xenopus embryos. Development *126*, 4715–4728.

Dubaissi, E., Rousseau, K., Lea, R., Soto, X., Nardeosingh, S., Schweickert, A., Amaya, E., Thornton, D.J., and Papalopulu, N. (2014). A secretory cell type develops alongside multiciliated cells, ionocytes and goblet cells, and provides a protective, anti-infective function in the frog embryonic mucociliary epidermis. Development *141*, 1514–1525. https://doi.org/10.1242/dev.102426.

Haas, M., Gómez Vázquez, J.L., Sun, D.I., Tran, H.T., Brislinger, M., Tasca, A., Shomroni, O., Vleminckx, K., and Walentek, P. (2019). ΔN-Tp63 mediates wnt/β-catenin-induced inhibition of differentiation in basal stem cells of mucociliary epithelia. Cell Rep. *28*, 3338–3352.e6. https://doi.org/10.1016/j.celrep.2019.08.063.

Icha, J., Weber, M., Waters, J.C., and Norden, C. (2017). Phototoxicity in live fluorescence microscopy, and how to avoid it. BioEssays *39*, 1700003. https://doi.org/10.1002/bies.201700003.

Kulkarni, S.S., Griffin, J.N., Date, P.P., Liem, K.F., and Khokha, M.K. (2018). WDR5 stabilizes actin architecture to promote multiciliated cell formation. Dev. Cell *46*, 595–610.e3. https://doi.org/10.1016/j.devcel.2018.08.009.

P.D. Nieuwkoop, J. Faber, J. Gerhart, and M. Kirschner, eds. (2020). Normal Table of Xenopus Laevis (Daudin): A Systematical and Chronological Survey of the Development from the Fertilized Egg till the End of Metamorphosis (Garland Science). https://doi.org/10.1201/9781003064565.

Quigley, I.K., Stubbs, J.L., and Kintner, C. (2011). Specification of ion transport cells in the Xenopus larval skin. Development *138*, 705–714. https://doi.org/10.1242/dev.055699.

Sedzinski, J., Hannezo, E., Tu, F., Biro, M., and Wallingford, J.B. (2017). RhoA regulates actin network dynamics during apical surface emergence in multiciliated epithelial cells. J. Cell Sci. *130*, 420–428. https://doi.org/10.1242/jcs.194704.

Sedzinski, J., Hannezo, E., Tu, F., Biro, M., and Wallingford, J.B. (2016). Emergence of an apical epithelial cell surface in vivo. Dev. Cell *36*, 24–35. https://doi.org/10.1016/j.devcel.2015.12.013.

Shaidani, N.-I., McNamara, S., Wlizla, M., and Horb, M.E. (2021). Obtaining Xenopus laevis embryos. Cold Spring Harb. Protoc. *2021*. pdb.prot106211. https://doi.org/10.1101/pdb.prot106211.

Sive, H.L., Grainger, R.M., and Harland, R.M. (2000). Early Development of Xenopus laevis: A Laboratory Manual (CSHL Press).

Stubbs, J.L., Davidson, L., Keller, R., and Kintner, C. (2006). Radial intercalation of ciliated cells during Xenopus skin development. Development *133*, 2507–2515. https://doi.org/10.1242/dev.02417.

Szabó, A., Cobo, I., Omara, S., McLachlan, S., Keller, R., and Mayor, R. (2016). The molecular Basis of radial intercalation during tissue spreading in early development. Dev. Cell *37*, 213–225. https://doi.org/10.1016/j.devcel.2016.04.008.